



HAL
open science

Evaluation of the strain-induced martensitic transformation by acoustic emission monitoring in 304L austenitic stainless steel: Identification of the AE signature of the martensitic transformation and power-law statistics

Maher Shaira, Nathalie Godin, Philippe Guy, L. Vanel, Joel Courbon

► To cite this version:

Maher Shaira, Nathalie Godin, Philippe Guy, L. Vanel, Joel Courbon. Evaluation of the strain-induced martensitic transformation by acoustic emission monitoring in 304L austenitic stainless steel: Identification of the AE signature of the martensitic transformation and power-law statistics. *Materials Science and Engineering: A*, 2008, pp.392-399. 10.1016/j.msea.2008.04.068 . hal-00433953

HAL Id: hal-00433953

<https://hal.science/hal-00433953>

Submitted on 18 Jan 2022

HAL is a multi-disciplinary open access archive for the deposit and dissemination of scientific research documents, whether they are published or not. The documents may come from teaching and research institutions in France or abroad, or from public or private research centers.

L'archive ouverte pluridisciplinaire **HAL**, est destinée au dépôt et à la diffusion de documents scientifiques de niveau recherche, publiés ou non, émanant des établissements d'enseignement et de recherche français ou étrangers, des laboratoires publics ou privés.



Distributed under a Creative Commons Attribution - NonCommercial 4.0 International License

Evaluation of the strain-induced martensitic transformation by acoustic emission monitoring in 304L austenitic stainless steel: Identification of the AE signature of the martensitic transformation and power-law statistics

M. Shaira^{a,c}, N. Godin^{a,*}, P. Gu[†], L. Vanel^b, J. Courbon^a

^a Université de Lyon, INSA-Lyon, MATEIS CNRS UMR 5510, 7 avenue J. Capelle, F-69621 Villeurbanne, France

^b Université de Lyon, Ecole Normale Supérieure de Lyon, Laboratoire de physique, CNRS UMR 5672, 46 allée d'Italie, F-69364 Lyon Cedex 07, France

^c Faculty of Mechanic and Electricity, University of Al-Baath, Homs, Syria

The aim of the present investigation is to characterize plasticity-induced martensite formation of metastable austenitic stainless steel at room temperature. Acoustic Emission (AE) monitoring is performed on a 304L austenitic stainless steel during fatigue tests. This work aims at identifying the acoustic emission signals associated with the formation of the strain-induced martensite. The present work includes the study of the influence of the specimen geometry. The use of statistical pattern recognition allowed the identification of the acoustic emission signatures for three mechanisms: dislocation motion, mechanical damage and martensitic transformation (MT). Moreover statistics on the energies of the AE signals were found to obey power laws ($P(E) \sim E^{-\alpha}$) with exponent $\alpha = 1.75 \pm 0.15$ for the cluster associated with martensite formation.

1. Introduction

The austenitic phase of some stainless steels is metastable at room temperature, such as that of 304L alloy. Martensitic transformation (MT) γ austenite $\rightarrow \alpha'$ bcc to slightly tetragonal martensite can be induced by quenching or by plastic deformation. By quenching the process starts at temperature M_s . Transformation can also occur above M_s under the influence of mechanical stresses and strains [1–12]. Cyclic strains also induce some MT. Since the displacive MT modifies the volume (with $\gamma \rightarrow \alpha'$ martensite a volume expansion occurs [2]), internal stresses are generated that can affect the lifetime of components subjected to fatigue. Thus the monitoring of MT is of societal interest and many non-destructive techniques have been applied, among which eddy current testing [13,14] and acoustic emission [15,16]. The aim of this study is to investigate MT by AE and MT in 304L steel during fatigue tests, using two kinds of analysis: pattern recognition and power-laws statistics, which we shortly describe hereunder.

2. Acoustic emission and martensitic transformation

It is well known for a long time that martensite formation in steels can be detected by AE monitoring [17,18]. Since then considerable work has been carried out to relate the detected AE signals to the kinetics of the martensitic transformation [19,20]. The AE of the thermally induced MT has been more frequently investigated [21–23] in the literature than that of the strain-induced MT. The acoustic emission (AE) technique is an efficient way to monitor damage growth in both laboratory specimens and structural components. It deals with the analysis of transient elastic waves generated by a sudden release of energy from localised sources within a material. Sensors set on the specimen surface capture these waves. Then, the recorded signals depend jointly on the events they originate from, and on the elastic and damping properties of the propagation medium and the sensor features. Thus, there is no universal signature of AE events. However, in permanent set-up conditions, similarities exist among AE signals originating from similar events. In the case of ASI 304L steel, many mechanisms during fatigue tests have been confirmed as AE sources including dislocation motion, formation of martensite, twin formation, inclusion fracture, crack nucleation and propagation. Then, discriminating the types of source mechanisms responsible for the detected AE signals is an exciting challenge. Indeed, it could allow to continuously monitor the damage progression in vulnerable

* Corresponding author. Tel.: +33 472438073; fax: +33 472437930.
E-mail address: nathalie.godin@insa-lyon.fr (N. Godin).

components. However, two main reasons make the discrimination of the AE mechanisms a non-trivial task. On one hand, the AE signals are complex objects that must be characterized by multiple pertinent descriptors in order to be processed. On the other hand, the acoustic signatures of AE events are not known *a priori* and they are rather scattered due to their sensitivity to the above-mentioned conditions. Consequently, AE signals collected from tests performed in actual conditions must be segmented into clusters based on closest similarities [24–26]. Any AE signal can be represented in an n -dimensional space by a vector which components are the signal descriptors. Cluster analysis partitions the input data space into k regions based on the distances between objects. The number k of clusters may or may not be known *a priori*. Depending on whether the cluster features are known or not, the classification algorithms are said supervised or unsupervised, respectively. In the case of AE data set, features of signal clusters are not available and unsupervised classifiers have to be used in order to search for them in the structure of the data set itself. The k -means algorithm [26,27] is one of the most widely used methods to determine cluster solutions for a particular user-defined number of clusters.

Power law distributions of event sizes are usually observed in physical systems close to the critical point of a second order phase transition. However, power-law behaviour can also occur in driven physical systems with intrinsic disorder, even when the physical process involves a first-order transition. Experimental observations of this kind have been reported for a large variety of phenomena such as earthquakes, martensitic transformation, Barkhausen noise, or rupture [28–31]. In some cases, it has been suggested that such systems follow the theory of Self-Organized Criticality (SOC) and thus evolve until a critical state is reached. Then events occur in avalanches showing no characteristic temporal and spatial scales. An important feature of such systems is that they respond to external perturbations by avalanche of all sizes S with a power law distribution $P(S) \sim S^{-\tau}$ where τ is a scaling exponent. A martensitic transformation is a diffusionless first-order phase transition. It involves a cooperative and almost simultaneous movement of atoms from parent to product phase. In athermal martensite, the martensite phase nucleates from isolated regions which are usually defects like dislocations or grain boundaries. Thus quenched disorder plays an important role in the initial kinetics of athermal martensite. The avalanche size distributions have been mostly investigated through the amplitude and duration of the peaks in acoustic emission signals [31,32]. The important result is that both quantities exhibit power-law distributions. This is an indication that the system evolves without characteristic time and length scales which is a typical feature of criticality. Vives et al. [31] have characterized the avalanche distributions during a thermally induced thermoelastic martensitic phase transition of a Cu–Zn–Al alloy, using AE techniques and shown it exhibits power-law behaviour for more than one decade. They obtained the exponents for the distributions of amplitudes $P(A) \sim A^{-\gamma}$, $\gamma = 3.6 \pm 0.8$ and durations $P(D) \sim D^{-\tau}$, $\tau = 3.5 \pm 0.8$. On the other hand, for stress-induced transformation, Carrillo et al. obtained $\gamma = 2.3 \pm 0.2$ [32]. In the study of dynamical systems, dissipated energy is usually used as a universal and relevant parameter to characterize the size of an instability. The energy E involved in the process is proportional to the square of amplitude, so these studies would lead to energy distributions $P(E) \sim E^{-\alpha}$ with the following expected values of α ($\alpha = (1 + \gamma)/2$): $\alpha = 2.3 \pm 0.4$ for thermal cycling [31] and $\alpha = 1.65 \pm 0.1$ for stress cycling [32]. More recently, a theoretical work [33] has been able to reproduce the magnitude of the exponent for thermal cycling but there is no model that can account for the exponent observed in stress cycling yet.

Table 1
Chemical composition of the 304L steel (wt%)

C	0.028
Si	0.490
Mn	1.40
P	0.034
S	0.017
Cr	18.21
Mo	0.46
Ni	8.15
Co	0.11
N	0.045

3. Material and experiments

The material studied in this work is a commercial 304L austenitic stainless steel, previously monitored by Pasco et al. [34] by Barkhausen noise (same batch of material). The material alloy is supplied in the form of a bar, 20 mm in diameter. The chemical composition of the material is given in Table 1. In order to obtain a homogeneous microstructure the material is annealed above 1000 °C during about 1 h and quenched in water. After this treatment, X-ray diffraction enabled to detect 15% of a bcc phase which can be a mixture of ferrite and martensite and 85% of the austenite (for low carbon contents, martensite has bcc structure). The resulting mean grain size is about 50 μm . An estimate of the temperature at which plenty of strain-induced martensite forms is the M_{d30} temperature, corresponding to the temperature at which an actual 30% strain induces the formation of 50% of martensite α' . The Pickering relation (1), given in mass percentage, enables to estimate M_{d30} from the steel composition [34–36]:

$$M_{d30} = 497 - 13.7\text{Cr}\% - 20\text{Ni}\% - 8.1\text{Mn}\% - 9.2\text{Si}\% - 462(\text{C} + \text{N})\% - 18.5\text{Mo}\% \quad (1)$$

For the studied steel, the application of the Pickering relation gives a M_{d30} equal to 26 °C which indicates that a martensitic transformation can appear under cyclic loading at room temperature. The dimensions of the fatigue specimen are shown in Fig. 1. Specimens with a cylindrical gauge length of 20 mm and a diameter of 4 mm are machined from the bars. Moreover specimens with a rectangular gauge length of 20 mm are tested in order to allow eddy current measurements [37,38].

Low cycle fatigue tests are performed with alternating load ($R = -1$) at room temperature on a 10 kN hydraulic testing machine. The fatigue tests are carried out under stress control at imposed maximal stress σ_{max} equal to 500 MPa, 600 MPa and 700 MPa with a frequency of 0.25 Hz, 0.166 Hz and 0.0121 Hz. The yield strength of the material is in a range 350–400 MPa. There is a soft transition between elasticity and plasticity for such a material. The strain is continuously measured throughout the test by an extensometer with 8 mm gauge length clamped to the specimen.

Metallography is performed on cuts of fatigue specimens. They are first ground on silicon carbide paper using 80, 180, 400 and 1200 grit. Specimens are further polished with 3 μm diamond paste. The chemical etching is mainly made by dipping the sample in an oxalic acid solution in order to reveal the austenitic grain structure including twins, slip bands and martensite. The microstructure of the materials is shown in Fig. 2a. After the fatigue tests the specimens are sectioned parallel and perpendicular to the stress axis. Twins are detected in the specimen before testing.

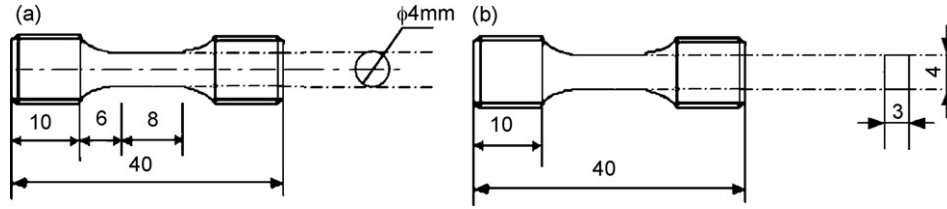


Fig. 1. Fatigue samples with a gauge length having (a) a circular section and (b) a rectangular section (mm).

4. Acoustic emission technical features

4.1. Acoustic emission monitoring

A two channel Mistras 2001 data acquisition system of Physical Acoustics Corporation (PAC) with a sampling rate of 8 MHz and a 40 dB pre-amplification is used to record AE data. The total amplification of the recording system is 80 dB. AE measurements are achieved by using two micro-80 PAC sensors, coupled on the samples with a thin layer of vacuum grease. The sensors are mounted on both heads of the specimens and are held in place with a mechanical device. The amplitude distribution covers the 0–100 dB range (0 dB corresponds to 1 μ V at the transducer output). It is very important to eliminate the acoustic emission originating from noise. Noise is created by the testing machine and the specimen grips. Electronic noise can also occur. So several precautions are taken to avoid extraneous acoustic noise. First, the amplitude threshold is set at 32 dB above ambient noise. Secondly, the AE hits which have frequency up to 900 kHz and with number of counts below 3 are eliminated. After installation of the transducers, a pencil lead break procedure [39] is used to generate repeatable AE signals for the calibration of each test. So, the acquisition parameters have been set as follows: peak definition time (PDT) = 300 μ s, hit definition time (HDT) = 600 μ s and hit lock time (HLT) = 1000 μ s. The attenuation is small enough to avoid doing any correction of the measured amplitudes. After the calibration step, AE is continuously monitored during tensile tests. Several parameters are calculated for each signal from the waveforms such as amplitude, duration, rise time, counts, counts to peak, frequency and energy. These parameters are collected as the components of an input vector X describing the signal they derive from.

4.2. Data clustering: *k*-means method

Nine reliable parameters or descriptors have been retained on account of the waveform diversity to describe an AE signal: ampli-

tude, duration, rise time, counts, counts to peak, energy, average frequency, initiation frequency and reverberation frequency. Initiation frequency is the ratio between the number of counts before the maximal amplitude and the rise time. Reverberation frequency is the ratio between the counts after the maximal amplitude and the decrease time. Moreover, among an AE data set, each descriptor is normalised by its variance in the range (0–1). This normalisation confers the same importance to each descriptor in the classification process. Then, a nine-component descriptor vector represents each AE signal. The *k*-means algorithm divides out an input data set among a predefined number of clusters k . The classification criterion is then the minimisation of the sum of the squared distances between all the descriptor vectors of a cluster and its centre. The clustering is run 15 times and only the best result is saved. The procedure is described in previous papers [25,26]. The *k*-means algorithm can then be summarised as follows:

1. Initialise the co-ordinates X_i of the cluster centre for each class C_i .
2. Assign each descriptor vector X to a class C_i such as the Euclidean distance between X and the cluster centre X_i should be the lowest among all the cluster centres.
3. Compute the co-ordinates of the new cluster centres.
4. If there is no change in the co-ordinates of the cluster centres, then the algorithm has converged and the procedure is terminated; otherwise go to step 2.

4.3. Power-laws statistics

In this study, we focus on the analysis of the energy distribution $P(E) \sim E^{-\alpha}$. These distributions have been computed using logarithmically spaced bins in order to increase the range of energy accessible in the statistical analysis. The exponent α has been estimated using a power law fit of the data and the error on the slope is given for a 90% confidence interval that is based on the dispersion of the data around the fit. In several instances, a power

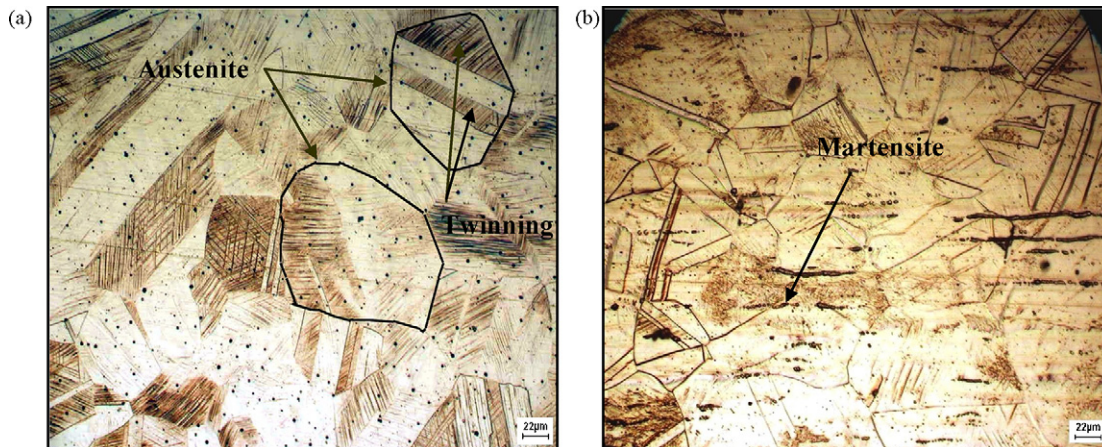


Fig. 2. Microstructure observed on the longitudinal cut of a fatigue specimen: (a) before fatigue test and (b) after failure ($\sigma_{\max} = 600$ MPa, $N = 605$).

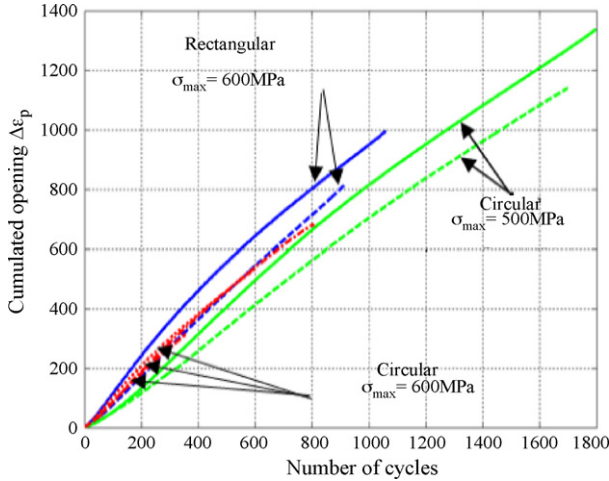


Fig. 3. Cumulated opening $\Delta\epsilon_p$ versus number of cycles for fatigue tests for seven samples.

law behaviour could be observed only for a restricted range of energy.

5. Results and discussion

5.1. Global behaviour: influence of the sample geometry

As expected from any Wöhler curve, the number of cycles at failure N_f drastically decreases with the increase of maximum applied load σ_{max} . Anyhow, N_f is also affected by sample geometry: under the same σ_{max} , samples with rectangular section tend to break above samples of circular section. They also induce more cyclic dissipation as shown by the plastic strain amplitude evolution over the trial, Fig. 3. Fig. 4(a) and (b) shows the cumulated AE energy versus the number N of cycles recorded at $\sigma_{max} = 600$ MPa for both types of

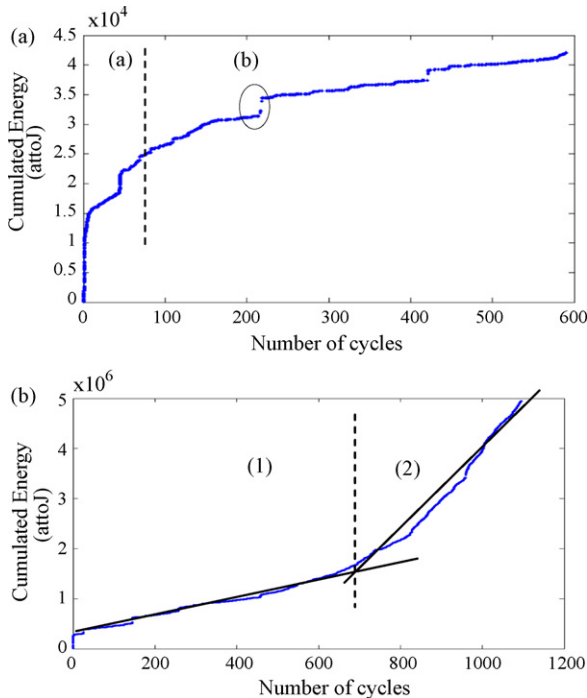


Fig. 4. Cumulative AE energy versus number of fatigue cycles: (a) circular section $\sigma_{max} = 600$ MPa, $N_f = 605$ and (b) rectangular section $\sigma_{max} = 600$ MPa, $N_f = 1062$.

specimens. Different behaviours can also be observed on cumulated release of AE energy. For the samples with circular section, during a first stage, the AE energy increases steadily; in a second stage, the activity globally decreases while presenting sudden bursts. The transition occurs at about $N = 70$ cycles. These global behaviours are very reproducible for several tests conducted under the same conditions. Indeed, the transition occurs when about 10% of the fatigue life has been spent. Shortly before fracture, there is a very slight increase of activity. On the other hand, for the samples with rectangular section, AE energy increases smoothly with the number of cycles and the activity accelerates during the second stage, the limit between stages occurring at about 50% of the lifetime. Fig. 2b shows the typical microstructure of a fatigue specimen. The distribution of the martensite laths in the austenitic matrix is found to be non-homogeneous. They form in the deformed austenite grains, in twins and near the cracks. In a plane perpendicular to the stress axis, there is more MT close to the free surfaces of the samples than in the bulk. When comparing rectangular and circular sections, there is also more MT in the corners. Orders of magnitude have been provided by X-ray diffraction analysis combined with eddy current measurements, which will be described in a forthcoming paper [40]. The main features are 24% transformation in bulk, 34% close to the surface and 48% in the corners in such conditions. The given concentrations are the values of the total concentrations of the bcc phases after the test. In a plane parallel to the stress axis, the distribution of martensite is lower in the middle of the gauge length and increases near the shoulders which correspond to the failure zone. For the cylindrical section, the martensite is also concentrated in shoulders. In this area, one finds also a large number of microcracks. The MT is strongly influenced by the geometry of the sample. It is heterogeneous and very sensitive to strain gradients: vicinity of free surfaces, or shoulders, or microcracks. The role of strain gradients is not evidenced by the way M_{d30} is obtained (monotonous tensile strain).

5.2. Pattern recognition (PR) analysis

From previous work reported in the literature [41], one would expect AE from initiation of dislocation slip if it produces dislocation avalanche but not simply from dislocation slip itself. The packet or avalanche of moving dislocations must glide far enough at sufficient velocity for the elastic waves to be detected. It is likely to correspond to fairly long AE events. Another source of AE is twinning, which would produce high amplitude AE bursts. It is difficult to ascertain that twinning did not occur at all during testing, but this mechanism contribution is certainly very low. Indeed, metallographic observations did not reveal more twinning at the end of the test MT, like twinning, is a displacive transformation of velocity close to sound speed [42]. Anyhow, the formation of a fine lath is likely to induce a very small release of energy. So one would expect brief bursts with little released energy. Finally the formation of microcracks as seen in metallography is also going to produce AE bursts in a range of energy depending on the size of the crack. So the postulated sources of AE are: (1) cooperative dislocation motion, (2) martensitic transformation and (3) mechanical damage such as crack initiation and propagation. The AE signals have thus been classified into three clusters by using the k-means pattern recognition method. Table 2 summarizes the mean characteristics of the obtained clusters of AE signals. The three clusters are always present and have the same mean characteristics independently of the gauge length shape. The segmentation of the AE data is very reproducible. From the AE distributions obtained after pattern recognition, some important differences in the AE signals characteristics are found. Indeed, three types of signals are identified to be distinct. Cluster 1 signals have a low frequency with a long rise time.

Table 2
AE parameters for the three clusters and a schematic representation of the waveform

Cluster	Rectangular section	Circular section	Schematic representation of the signal
1			
Rise time (μs)	72	94	
Amplitude (dB)	37	44	
Duration (μs)	326	324	
Av. frequency (kHz)	61	63	
Energy (aJ)	16	87	
2			
Rise time (μs)	28	15	
Amplitude (dB)	45	50	
Duration (μs)	423	243	
Av. frequency (kHz)	142	143	
Energy (aJ)	226	559	
3			
Rise time (μs)	1	1	
Amplitude (dB)	40	47	
Duration (μs)	133	102	
Av. frequency (kHz)	112	140	
Energy (aJ)	20	137	

Cluster 2 signals have a shorter rise time with a higher frequency. The last cluster is constituted by very short signals. Cluster 3 corresponds to almost impulse signals. Fig. 5 shows the projection of the classified signals onto the ratio amplitude/rise time versus average frequency plane. The three clusters are easily distinguishable on this plane, which means the PR algorithm succeeded in creating compact and well-separated clusters.

5.3. Clusters labelling

The resulting clusters should now be correlated with the different AE mechanisms. We assume that the AE energy is proportional to the energy dissipated at the AE source whatever the source mechanism. Detectable AE bursts release a sufficient amount of energy in a short period of time. The faster the fracture process, the more the stress wave should look like a delta-pulse. The cumulative energy as well as the AE rate for each of the three clusters versus the number N of cycles is presented in Fig. 6 for samples with circular section and in Fig. 7 for samples with rectangular section. According to these plots, the difference between each cluster AE response is strongly affected by the geometry. For circular sections as shown in Fig. 6, initially Clusters 1 and 2 are dominant. Energy release of Cluster 1 is very active at the beginning of the test during the first cycles. But at the end of the test, this cluster contains less than 30% of cumulated AE energy. As for the AE rate, this cluster is active throughout the test. Cluster 2 is increasingly activated as the test proceeds, reaching about 40% of the total number of signals and 60% of the total AE energy. Cluster 3 is not energetic (less than 10% of the total energy) and gets activated by

sudden bursts. For rectangular sections as shown in Fig. 7, Clusters 1 and 2 present the same chronology of activation in term of energy and number of signals, characterized by a break of slope at about half the lifetime. It is observed that Clusters 1 and 2 are characterized by a high activity during the first cycle and next during the second part of the test. With increasing number of cycles, class 2 increased, reaching about 40% of the total in term of number of signals and 90% in term of AE energy. Again, the activation of Cluster 3 appears significantly different from that of Clusters 1 and 2.

5.3.1. Cluster 1

The analysis of the AE Cluster 1 shows that the AE is basically of continuous type and the emission is composed of a very large amount of low energy, low frequency and long rise time signals. It is very active during the first cycle, as shown in Figs. 6a and 7a. This is consistent with the emission being generated by collective dislocation motion, very large during the first cycles due to overall plasticity. The decrease in AE activity of Cluster 1 (Figs. 6a and 7a) after the first cycle can then be linked with dislocation storage that reduces the mean free path of mobile dislocations, thus reducing the statistical probability of detection of weak AE phenomena. The higher activity of the rectangular sections is a consequence of their higher plastic strain amplitude during the trial (Fig. 3). Indeed, it cannot be excluded that additional contributions arise from twinning, as well as from dislocation activity in front of crack tips and even indirectly from martensitic transformation through dislocation strengthening, that is through the motion of the additional free dislocations created in surrounding ferrite [43].

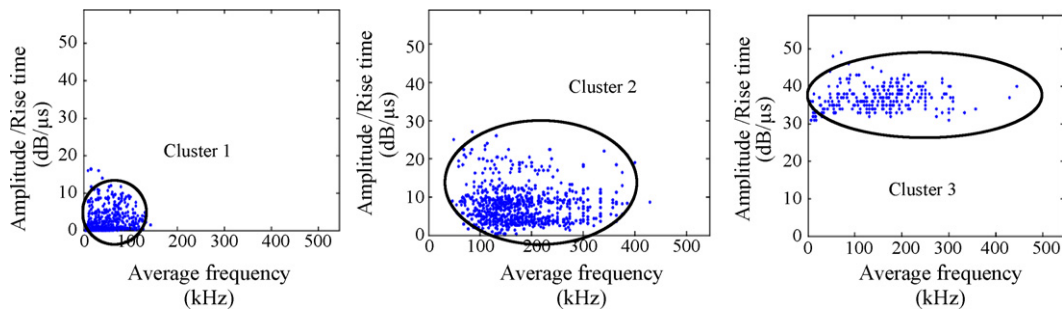


Fig. 5. Clustering results in a 2D projection: amplitude/rise time ratio versus average frequency scatter plot for the three clusters identify on sample with circular section.

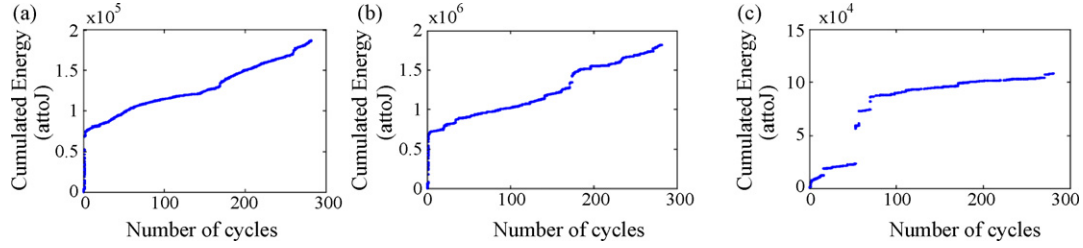


Fig. 6. Evolution of the number of hits of each clusters versus number of cycles: (a) Cluster 1, (b) Cluster 2 and (c) Cluster 3. Sample with circular section $\sigma_{\max} = 700$ MPa, $N_f = 281$ cycles.

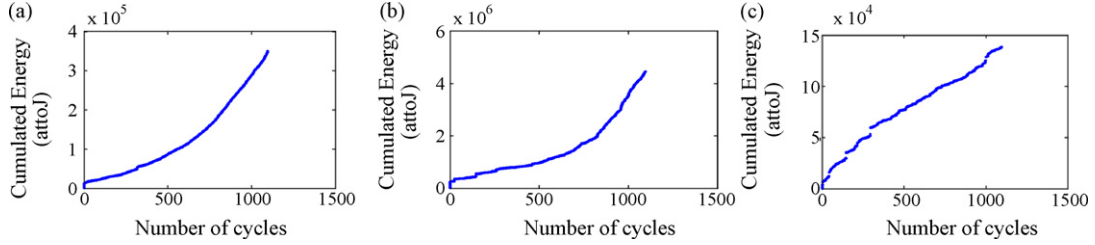


Fig. 7. Evolution of the number of hits of each clusters versus number of cycles: (a) Cluster 1, (b) Cluster 2 and (c) Cluster 3. Sample with rectangular section $\sigma_{\max} = 600$ MPa, $N_f = 1062$ cycles.

5.3.2. Cluster 2

A rapid crack growth produces signals with short rise time and high energy. Cluster 2 is the most energetic, containing short high-frequency bursts, releasing locally an important power. The crack lips can rub against each other in the compression phases, thus generating more AE. Indeed, Cluster 2 is also activated during the unloading and the compressive phase [38]. Moreover it has a strong activity at the end of the tests. All these arguments are coherent with the attribution of Cluster 2 to cracking phenomena. An objection could be the important release of energy at the beginning of the test. Yet the plastic strain amplitude is high: about 0.5%, so that mechanical damage can readily occur from the very beginning of the test.

5.3.3. Cluster 3

Concerning the formation of α' -martensite, there is a good agreement in the literature that nucleation occurs preferentially at intersecting shear band [2,44] so without mechanical damage. Bayerlein [2] showed that threshold plastic strain amplitude must be exceeded to trigger the formation of martensite; he found around 0.3%. This result was reported by other authors [7,11]. In our case the plastic strain amplitude is around 0.5% so the TM can occur from the beginning of the test [34]. Moreover, Mohr and Mukherjee [45] showed that in fully austenitic steels, the energy of acoustic emission generated during martensitic transformation is proportional to the volume of transformed regions. The martensite laths we observed is very fine so that the expected released acoustic energy accompanying MT is weak but intense, due to the displacive character of MT [42]: TM should produce delta like signals. Indeed, the analysis of the AE Cluster 3 shows that the emission is composed of very short signals. Fig. 8 shows the evolution of the energy of the Cluster 3 versus the martensite volume fraction at the end of the test obtained with different samples. The energy involved in the Cluster 3 seems to be proportional to the rate of MT. If we attribute Cluster 3 to MT, it then starts at small number of cycles for each specimen. It is consistent with the results obtained by Pasco et al. using Barkhausen noise on the same batch of material [34]. The extrapolation of the line given in Fig. 8 starts at (15%, 0) which corresponds to the initial bcc proportion phase in the sample. They showed that the martensitic transformation starts from the first

cycle. Then at a threshold value of the number of cycles around 70 (Fig. 6c), a large amount of energy is released in one or few events. In this scenario, the amount of transformation at a given number of cycles is proportional to the overall energy released by the sample in Cluster 3. The remaining transformation is completed gradually, by relatively small events. The kinetic of the transformations actually differ for each type of sample section. For rectangular sections, the activity of the Cluster 3 in terms of both energy and number of signals increases linearly with the number N of cycles. In this sample, almost all transformation is completed gradually by small events. This result is in agreement with previous works [1,11,14]. Kalkhof showed that for the given material and loading conditions the volume fraction of martensite depended on the cycle number. Indeed, a linear relationship between the volume fraction of martensite measured by eddy-current and the number of cycles is determined. Moreover, the fact that MT starts quickly for the sample with rectangular section is coherent with the early transformation in the edges and close to the plane surfaces of this kind of specimen. The geometry of the samples as well as the variability of the results show that the kinetics of the MT is variable.

5.4. Power-laws statistics

The first result of the present analysis is that the probability density function of the AE event energies obeys a power law dis-

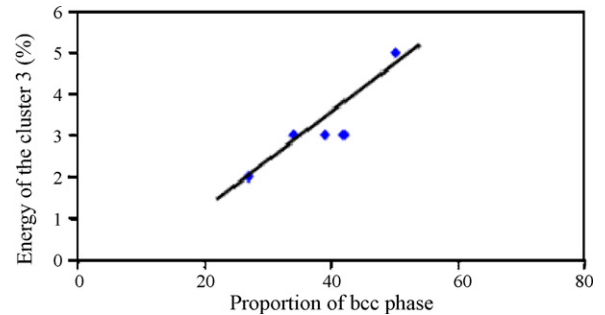


Fig. 8. Energy of the Cluster 3 versus proportion of bcc phase. Sample with circular section.

tribution independently of the maximum applied stress and the sample geometry. The release of energy during the test follows a power law and this over several decades. An exponent range from 1.4 to 1.7 was obtained whatever the shape of the sample and the applied load. Here, no distinction between dislocations, cracking and MT is done as if these phenomena belonged to the same global dynamics. To go beyond this simple analysis, we consider separately the data corresponding to each cluster. The change in $P(E)$ depending on the cluster as seen in Fig. 9 is particularly remarkable. Fig. 9 shows the energy distribution for samples of cylindrical section. Similar results were obtained with rectangular section. Although chronologies of activation of the three classes are different for the two geometries, the power law behaviour is independent of the geometry of the sample. Globally, the distributions are power law with different slopes depending on the type of cluster. In Fig. 9a, for Cluster 1, we find $\alpha = 2.14 \pm 0.18$ above $E \approx 100$ aJ. We remind that Cluster 1 was associated with dislocation motion and twinning. Distribution of acoustic energies associated to dislocation motion have been studied in other systems such as ice and metallic single crystals and also ice polycrystals. In single crystals, an exponent close to 1.5 [46,47] is observed while in polycrystals the exponent can be smaller, around 1.2 [48]. In polycrystals, it is argued that the smaller exponent comes from the dislocation motion being hindered by the grain boundaries. Given the polycrystalline structure of 304L austenitic stainless steel, we could have expected to observe in Cluster 1 an exponent close to the one in ice polycrystals. In Fig. 9a, we observe a departure from power law behaviour at energies smaller than $E \approx 100$ aJ. The first thing that comes to mind is that this departure could be due to loss of small amplitude signals. If we extract anyway the typical power law slope of the distribution in this low energy range, excluding the behaviour at very low amplitudes, we find that $\alpha = 1.27 \pm 0.18$. We simply note that this value is not far from the exponent measured for ice polycrystals, and not so far from the exponent measured in ice or metallic single crystals. In Fig. 9b, we find for Cluster 2 a power law behaviour with a slope $\alpha = 1.31 \pm 0.04$ for a range of energies between 10 aJ and 1000 aJ. We associated Cluster 2 with mechanical damage such as cracks initiation, growth and coalescence. The power law that we find is consistent with distributions of acoustic energies measured during rupture of materials such as plaster or paper ($\alpha = 1.3$) [49,50], and not far from the slope observed for wood, fiber composites, dense polymer foams, or volcanic rocks ($\alpha = 1.5$) [28–30,51]. Note also that Minozzi et al. [52] have been able to model numerically the emergence of power law distribution for acoustic emission energies associated to rupture events, but have found a slightly higher value than most experiments ($\alpha = 1.7$). Above 1000 aJ in Fig. 9b, there is a change in slope ($\alpha = 1.99 \pm 0.17$) which is not necessarily a different power law behaviour but could simply come from a finite size effect cut-off of the largest events. However, both for Cluster 1 and Cluster 2, it is important to realize that the mean value of the acoustic energy in each cluster (see Table 2) is actually very close to the cut-off observed in the low energy range for Cluster 1 and in the high energy range for Cluster 2. This remark suggests that the restricted range of the power law behaviour at the cut-off values might have more physical meaning than being just an experimental limitation. For instance, in the case of dislocation motion, Ananthakrishna et al. [53] suggest that strong disorder can shift the dynamics away from criticality, thus making the range of the power law behaviour effectively smaller. Finally, as a side note, we observe that Cluster 1 and Cluster 2 have similar exponents both for the low and high energy ranges. In Fig. 9c, for Cluster 3 that was associated with MT, the distribution follows a power law for almost four decades in energy. From the linear fit shown in Fig. 9c we get $\alpha = 1.74 \pm 0.07$. The exponent found depends little on the shape of the sample or on the applied load. It is also remarkable that compared to Cluster 1

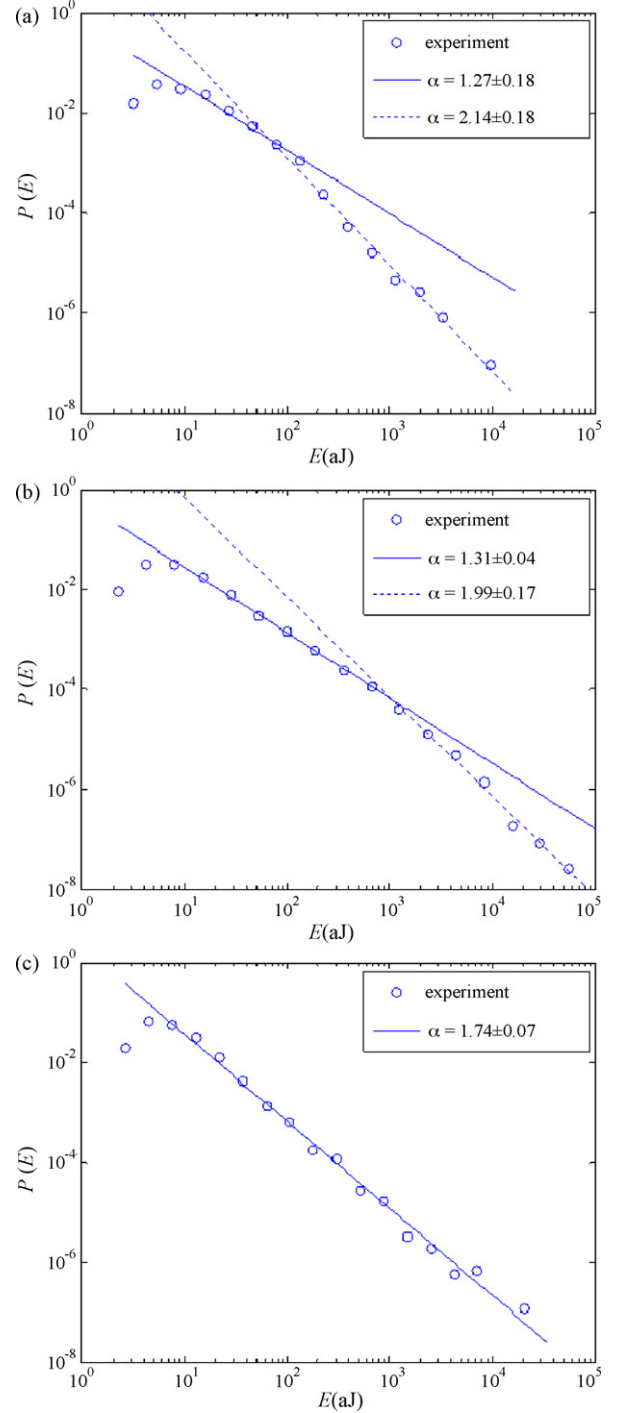


Fig. 9. Distributions of energies for the AE data of cluster: (a) 1 associated with dislocations, (b) 2 associated with cracking and (c) 3 associated with MT. Lines are power laws with exponents indicated above. Fatigue test on sample with circular section.

and 2, there is no experimental cut-off value in the distribution for Cluster 3. The reason for this lack of cut-off value is not clear at the moment. Overall, we can conclude for Cluster 3 that the AE energies distribution exponent shows a universal exponent 1.75 ± 0.15 independent of the sample's geometries and the stress amplitude. This value is in the same range than the one obtained in previous experimental studies [32] which reinforces the hypothesis that Cluster 3 is related to strain-induced MT. In [33], a model was proposed to explain the power law behaviour of acoustic emissions during ther-

mally induced MT. Although the theoretical value of the exponent is close to the one observed in thermal cycling experiments [31], there is currently no equivalent prediction for the case of strain-induced martensitic transformation, and especially for the value of the exponent.

In summary, taking into account the conclusions obtained from AE activity, each cluster has been correlated with a different AE mechanism as follows: (i) signals in Cluster 1 are assigned to dislocations; (ii) signals in Cluster 2 to mechanical damage and (iii) signals in Cluster 3 to martensitic transformation.

6. Conclusion

The low-cycle fatigue of 304L stainless steel was monitored by acoustic emission for two specimen geometries: a circular and a rectangular cross section. Both geometries exhibit a different lifetime and a different plastic strain amplitude, as well as a different AE behaviour.

The k-means method enabled to classify the AE signals into three clusters with marked features:

- Cluster 1 with lower frequency and with longer rise time resulted from dislocations movement;
- Cluster 2, the most energetic class, was associated with mechanical damage: crack activity;
- Cluster 3, whose signals are of impulse type, was associated with the martensitic transformation.

While the evolution of the activity of these clusters during the tests showed large differences, the statistical distribution of the energy within the classes did not depend on the geometry of the sample. Most remarkably, the statistical distribution of energies for the signals attributed to the martensitic transformation were found to follow a power law over four decades with no sign of cut-off. The exponent $\alpha = 1.75 \pm 0.15$ is coherent with previous experimental or theoretical works on critical dynamics.

Altogether, the k-means classification proved to be a powerful tool to find order or at least universality behind the apparent disorder of concurrent AE mechanisms.

References

- [1] M. Grosse, D. Kalkhof, M. Niffenegger, L. Keller, *Mater. Sci. Eng. A* 437 (2006) 109–113.
- [2] M. Bayerlein, H.-J. Christ, H. Mughrabi, *Mater. Sci. Eng. A* 114 (1989) L11–L16.
- [3] Th. Nebel, D. Eifler, *Sadhana-Acad. P. Eng. S.* 28 (2003) 187–208.
- [4] M. Botshekan, S. Degallaix, Y. Desplanques, *Mater. Sci. Eng. A* 234–236 (1997) 463–466.
- [5] S.S.M. Tavares, D. Gunderov, V. Stolyarov, J.M. Neto, *Mater. Sci. Eng. A* 358 (2003) 32–36.
- [6] W.-Y. Maeng, M.-H. Kim, *J. Nucl. Mater.* 282 (2000) 32–39.
- [7] U. Krupp, H.-J. Christ, P. Lezuo, H.J. Maier, R.G. Teteruk, *Mater. Sci. Eng. A* 319–321 (2001) 527–530.
- [8] W.-S. Lee, C.-F. Lin, *Scripta Mater.* 43 (2000) 777–782.
- [9] K.P. Staudhammer, L.E. Murr, S.S. Hecker, *Acta Metall.* 31 (1983) 267–274.
- [10] M. Grosse, D. Kalkhof, L. Keller, N. Schell, *Physica B* 350 (2004) 102–106.
- [11] M. Grosse, M. Niffenegger, D. Kalkhof, *J. Nucl. Mater.* 296 (1–3) (2001) 305–311.
- [12] P.L. Mangonon Jr., G. Thomas, *Metall. Trans. A* 1 (1970) 1577–1586.
- [13] M. Zergoug, S. Lebailli, H. Boudjellal, A. Benchaala, *NDT & E Int.* 37 (1) (2004) 65–72.
- [14] D. Kalkhof, M. Grosse, M. Niffenegger, H.J. Leber, *Fatigue Fract. Eng. M* 27 (2004) 595–607.
- [15] A.G. Beattie, *J. Acoust. Emiss* 2 (1/2) (1983) 95–128.
- [16] D.G. Eitzen, H.N.G. Wadley, *J. Res. Nat. Bur. Stand.* 89 (1) (1984) 75–100.
- [17] R.G. Liptai, H.L. Dunegan, C.A. Tatro, *Int. J. NDT* 1 (3) (1969) 213–221.
- [18] G.R. Speich, R.M. Fisher, *ASTM STP* 505 (1972) 140–151.
- [19] A. Planes, D. Rouby, J.L. Macqueron, M. Morin, G. Guenin, *J. Phys. D: Appl. Phys.* 15 (1982) 89–95.
- [20] L. Manosa, A. Planes, D. Rouby, M. Morin, P. Fleischmann, J.L. Macqueron, *Appl. Phys. Lett.* 54 (1989) 2574–2576.
- [21] S.M.C. Van Bohemen, M.J.M. Hermans, G. den Ouden, I.M. Richardson, *J. Phys. D: Appl. Phys.* 35 (2002) 1889–2189.
- [22] S.M.C. Van Bohemen, M.J.M. Hermans, G. den Ouden, *J. Phys. D: Appl. Phys.* 34 (2001) 3312–3317.
- [23] S.M.C. Van Bohemen, J. Sietsma, M.J.M. Hermans, I.M. Richardson, *Acta Mater.* 51 (2003) 4183–4196.
- [24] C.R.L. Murthy, B. Dattaguru, A.K. Rao, *J. Acoust. Emiss.* 6 (1987) 19–28.
- [25] N. Godin, S. Huguet, R. Gaertner, L. Salmon, *NDT & E Int.* 37 (2004) 253–264.
- [26] N. Godin, S. Huguet, R. Gaertner, *NDT & E Int.* 38 (2005) 299–309.
- [27] A. Likas, N. Vlassis, J. Verbeek, *Pattern Recogn.* 366 (2003) 451–461.
- [28] G. Durin, S. Zapperi, *Phys. Rev. Lett.* 84 (2000) 4705.
- [29] J.C. Anifrani, C. Le Floch, D. Sornette, D. Souillard, *J. Phys. I* 5 (6) (1995) 631–638.
- [30] S. Deschanel, L. Vanel, G. Vigier, N. Godin, S. Ciliberto, *Int. J. Fracture* 140 (2006) 87–98.
- [31] E. Vives, I. Rafols, L. Manosa, J. Ortin, A. Planes, *Phys. Rev. B* 52 (1995) 12644–12650.
- [32] L. Carrillo, J. Ortin, *Phys. Rev. B* 56 (1997) 11508–11517.
- [33] R. Ahluwalia, G. Ananthakrishna, *Phys. Rev. Lett.* 86 (2001) 4076.
- [34] L. Pasco, PhD thesis, Lyon, INSA de Lyon, France No. 04 ISAL 013, 2004.
- [35] A. Vincent, L. Pasco, M. Morin, X. Kleber, P. Donnadieu, *Acta Mater.* 53 (2005) 4579–4591.
- [36] T. Angel, *J. Iron Steel Inst.* (1954) 402–412.
- [37] M. Shaira, N. Godin, J. Courbon, P. Guy, *Proceedings of the 16th International Conference on Adaptive Structures and Technologies*, Published in Bookstore of "ICAST 2005 Sixteenth International Conference on Adaptive Structures and Technologies", Paris, October 9–12, 2005, DES tech Publications, USA, 2005.
- [38] M. Shaira, 2006, PhD thesis, Lyon, INSA de Lyon, France No. 2006-ISAL-0087.
- [39] A. Nielsen, *The Danish Welding Institute Publication*, 1980.
- [40] M. Shaira, P. Guy, J. Courbon, N. Godin, RNDE, submitted for publication.
- [41] J.R. Frederick, D.K. Felbeck, *ASTM STP* 505 (1972) 129–139.
- [42] H. Hallberg, P. Hakansson, M. Ristinmaa, *Int. J. Plasticity* 23 (2007) 1213–1239.
- [43] P. Jacques, Q. Furnemont, A. Mertens, F. Delannay, *Philos. Mag. A* 81 (2001) 1789–1812.
- [44] L.E. Murr, K.P. Staudhammer, S.S. Hecker, *Metall. Trans. A* 13A (1982) 627–635.
- [45] C. Tatro, A. Mukherjee, J. Mohr, *Mater. Eval.* 44 (9) (1986) 26–126.
- [46] M.C. Miguel, A. Vespignani, S. Zapperi, J. Weiss, J. Grasso, *Nature* 410 (2001) 667–671.
- [47] T. Richeton, P. Dobron, F. Chmelik, J. Weiss, F. Louchet, *Mater. Sci. Eng. A* 424 (2006) 190–195.
- [48] T. Richeton, J. Weiss, F. Louchet, *Acta Mater.* 53 (2005) 4463–4471.
- [49] A. Petri, G. Paparo, A. Vespignani, A. Alippi, M. Costantini, *Phys. Rev. Lett.* 73 (25) (1994) 3423–3426.
- [50] L.L. Salminen, A.I. Tolvanen, M.J. Alava, *Phys. Rev. Lett.* 89 (2002) 185503.
- [51] P. Diodati, F. Marchesoni, S. Piazza, *Phys. Rev. Lett.* 67 (1991) 2239.
- [52] M. Minozzi, G. Caldarelli, L. Pietronero, S. Zapperi, *Eur. Phys. J. B* 36 (2003) 203–207.
- [53] G. Ananthakrishna, C. Fressengeas, *Scripta Mater.* 52 (2005) 425–428.